

Optimal Joint Radar and Communication User Association in Cell-Free mMIMO Systems

Ahmed Naeem, El Mehdi Amhoud *Member, IEEE*, Hüseyin Arslan *Fellow, IEEE*

This work has been submitted to the IEEE for possible publication. Copyright may be transferred without notice, after which this version may no longer be accessible.

Abstract—The cell-free massive multiple-input multiple-output (CF-mMIMO) systems are crucial for 6G development due to their high spectral efficiency and uniform user-experienced data rates. A key aspect of CF-mMIMO is user association (UA) and optimal cluster formation. Traditional methods focusing solely on communication-related metrics fall short in this context, as sensing is becoming integral to 6G. This study delves into a framework for joint radar and communication (JRC) in CF-mMIMO systems and investigates JRC-based UA techniques. We propose a novel method to optimize UA, enhancing both communication spectral efficiency and sensing accuracy. Existing literature has not explored this dual requirement integration for UA. Our proposed two-step scheme optimizes UA clusters for both communication and sensing. The first step involves selecting access points (APs) based on channel quality, followed by a second step that further refines the selection by choosing APs from the initial group that are also optimal for sensing. We utilize the signal-clutter plus noise ratio to exclude APs with clutter in front of the user equipment (UE) and the AP view angle, ensuring that radar echoes are received only from the specific UE, not the surrounding clutter. Theoretical analysis and simulations demonstrate that the same APs optimized for communication are not necessarily optimal for sensing, highlighting the need for schemes that incorporate sensing requirements in UA. The results show the effectiveness of the proposed method, showing its potential to improve CF-mMIMO system performance in JRC scenarios.

Index Terms—Cell-Free mMIMO, clutter, joint radar and communication, sensing, spectral efficiency, user association.

I. INTRODUCTION

With the ever-growing connectivity, sixth generation (6G) will revolutionize networks by offering high data rates, ultra-low latency, and seamless connectivity through advancements like higher frequencies, massive multiple-input multiple-output (mMIMO), and intelligent network management. Furthermore, in conjunction with wireless communication developments, sensing will also play a pivotal role in enhancing 6G leading to the emergence of joint radar and communication (JRC), with many applications such as virtual reality, autonomous vehicles, and activity recognition [1]. Thus, integrating these technologies is crucial for realizing the full potential of 6G.

Building upon the above advancements, improving service quality and uniform data rates in future networks is pivotal.

Ahmed Naeem and Hüseyin Arslan are with the Department of Electrical and Electronics Engineering, Istanbul Medipol University, Istanbul, 34810, Turkey (email: ahmed.naeem@std.medipol.edu.tr, huseyin-arслан@medipol.edu.tr).

El Mehdi Amhoud is with the College of Computing, Mohammed VI Polytechnic University, Benguerir, Morocco (email: elmehdi.amhoud@um6p.ma).

Current networks achieve high peak data rates at cell centers but face substantial variations and inconsistent service quality at cell edges [2]. Despite deploying ultra-dense networks and mMIMO systems to enhance user-experienced data rates, challenges like significant signal-to-noise ratio (SNR) fluctuations and inter-cell interference persist [3]. Future networks should ensure consistent user-experienced data rates across the coverage area, not just increasing peak or average rates [4].

The cell-free mMIMO (CF-mMIMO) is a promising approach to address the challenges of inconsistent service quality and data rates faced by current networks. This technology combines aspects of both ultra-dense networks and mMIMO systems to ensure uniform data rates across the coverage area [5]. The main motivation is to enhance user-experienced data rates, rather than merely increasing peak rates [6]. A CF-mMIMO can be visualized as a network with a dismantled mMIMO array [7], where individual antennas are deployed at various locations. For a specific user equipment (UE), the distributed antennas transmit data signals with varying power and phase shifts, ensuring that the signals reach the UE synchronously and reinforce each other [4].

One of the critical factors in the effectiveness of CF-mMIMO is user association (UA) [8]. Unlike the conventional cellular networks where each UE is only associated with a single access point (AP), in CF-mMIMO each UE is served by a subset of access points (APs). Consequently, research in the field of UA in CF-mMIMO has gained significant attention for its potential to optimize UE and AP associations, thereby enhancing reliability, data rates, and overall system performance. When considering AP selection schemes in CF-mMIMO systems for communication-only fall into two categories: large-scale-based and competition-based schemes. In large-scale-based schemes, user equipments (UEs) select APs with the largest large-scale fading coefficient (LSFC) and better channel conditions. Each LSFC is sorted in order and compared to a threshold [4]. A user-centric virtual cell approach is introduced in [9], [10], where UA is done by considering the strongest channels (i.e., largest norm). Moreover, in [11] an AP selection scheme is introduced subject to reducing the backhaul requirements. A joint AP and UE preference-based scheme to ensure scalability for all UEs is proposed in [12]. Another association method is proposed in [13], which uses the Hungarian algorithm to create a cluster of APs to serve a UE based on their locations. Furthermore, in a competition-based scheme, a new accessing UE competes for an AP already serving its maximum number of UEs. The AP

prioritizes UEs with the best channel conditions by identifying the weakest UE it serves. If the new UE offers a better channel, it replaces the weakest one, which then blacklists the AP [4], [10].

All the aforementioned works primarily focus on associating UEs with APs from the perspective of communication-related service metrics only. However, to meet the dual needs of communication and sensing, new optimized UA schemes are required to enhance overall JRC network performance. For an optimized UA scheme in a JRC CF-mMIMO system, robust communication links are essential to achieve high data rates and reliable connectivity. Simultaneously, accurate sensing is vital for applications such as localization, target tracking, environmental monitoring, and autonomous systems. Therefore, integrating both aspects into UA strategies is crucial. Moreover, the CF-mMIMO architecture is particularly advantageous for multi-static sensing, providing high resolution, robust sensing, and a wider range of sensing angles [14]. Research on JRC in CF-mMIMO systems is limited, existing work mainly focuses on power allocation [14], [15], multi-target detection [16], [14], JRC beamforming [17], and defining communication and sensing regions [18]. Despite these research efforts, the field of JRC in CF-mMIMO systems remains an active area of investigation, with significant potential for further advancements.

To effectively address communication and sensing needs, this paper highlights a new approach for optimizing JRC-based UA in CF-mMIMO. The key contributions are

- 1) This paper proposes a JRC framework for CF-mMIMO systems, where each AP performs sensing and communication concurrently. The proposed framework provides a detailed step-by-step explanation of the signaling involved, offering a comprehensive understanding of the JRC CF-mMIMO architecture.
- 2) Unlike previous studies that have not integrated sensing requirements into CF-mMIMO UA, this paper proposes a novel two-step approach that combines both communication and sensing requirements. By jointly addressing these requirements, the proposed UA scheme aims to enhance the overall performance of the JRC CF-mMIMO systems.
- 3) This dual-step approach leverages signal-clutter plus noise power ratio (SCNR) to filter out APs from the cluster that are affected by significant clutter, ensuring precise radar echoes only from specific UE(s). The proposed scheme first selects APs based on channel quality and then refines this selection by considering APs that are also optimal for sensing. The paper also provides detailed optimization problems and corresponding algorithmic solutions to address this issue.
- 4) We analyze the communication spectral efficiency (SE), the impact of clutter on radar detection coverage probability (P_{dc}), and how different clutter densities and radar cross section (RCS) of the clutter affect the performance of the UA. A detailed mathematical analysis is provided in both line-of-sight (LoS) and non LoS (NLoS) radar echo reception in a cluttered environment and its impact on the performance of sensing and AP selection.
- 5) Moreover, we conduct detailed simulations and theo-

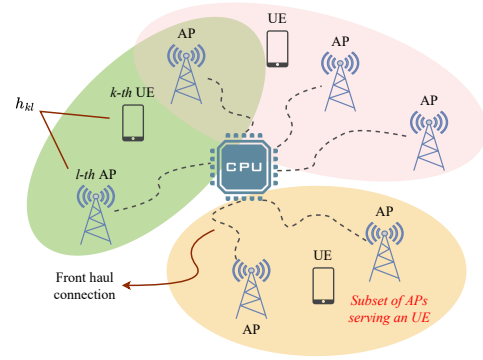


Fig. 1. Cell-Free mMIMO network.

retical analysis, including detailed mathematical evaluations, to assess the performance of the proposed UA scheme. The results show significant improvements in communication and sensing compared to traditional methods, validating the effectiveness of our approach. Our findings highlight the importance of accounting for sensing requirements in a cluttered environment to enable optimal UA decisions in the integrated JRC CF-mMIMO systems.

The paper is organized as: Section II presents the system model and framework of JRC CF-mMIMO. Section III formulates the optimization problems. The proposed UA method is detailed in Section IV, followed by the simulation results in Section V. Finally, Section VI concludes the paper.¹

II. SYSTEM MODEL

This section explains the JRC-based UA framework in CF-mMIMO, with a dual function radar communication (DFRC) [19], monostatic topology where a group of APs communicates with a UE while simultaneously sensing and tracking its movement [20]. Unlike [14], where each AP is either a JRC transmitter or a sensing receiver, our approach enables each AP to function as both, for better resources utilization.

A. Network Architecture

We consider a CF-mMIMO with K single-antenna UEs, $\mathcal{K} \triangleq \{1, 2, \dots, K\}$, and L randomly located APs with N antennas for 3D beamforming as [21] and [22]. All APs are connected via a front-haul to a central processing unit (CPU), as shown in Fig. 1. We assume a distributed implementation, following time division duplexing (TDD) protocols as illustrated in Fig. 2. The channel between the l -th AP and the

¹Notation: Boldface uppercase letters, \mathbf{X} , denote matrices, and boldface lowercase letters, \mathbf{x} , denote column vectors, Superscripts T , $*$, and H denote transpose, conjugate, and conjugate transpose, respectively. The entry (i, j) of matrix \mathbf{X} is $\mathbf{X}_{i,j}$, and $\mathbf{X}_{:,j}$ is its j -th column. The $n \times n$ identity matrix is \mathbf{I}_n . We use \triangleq for definitions and $\text{diag}(\mathbf{A}_1, \dots, \mathbf{A}_n)$ for a block-diagonal matrix with square matrices $\mathbf{A}_1, \dots, \mathbf{A}_n$ on the diagonal. The multivariate circularly symmetric complex Gaussian distribution with correlation matrix \mathbf{R} is denoted $\mathcal{N}_{\mathbb{C}}(\mathbf{0}, \mathbf{R})$. The Euclidean norm of \mathbf{x} is $\|\mathbf{x}\|_2$. The expected value of \mathbf{x} is $\mathbb{E}\{\mathbf{x}\}$. We denote the cardinality of set \mathcal{A} by $|\mathcal{A}|$ and its n -th element by $\mathcal{A}(n)$.

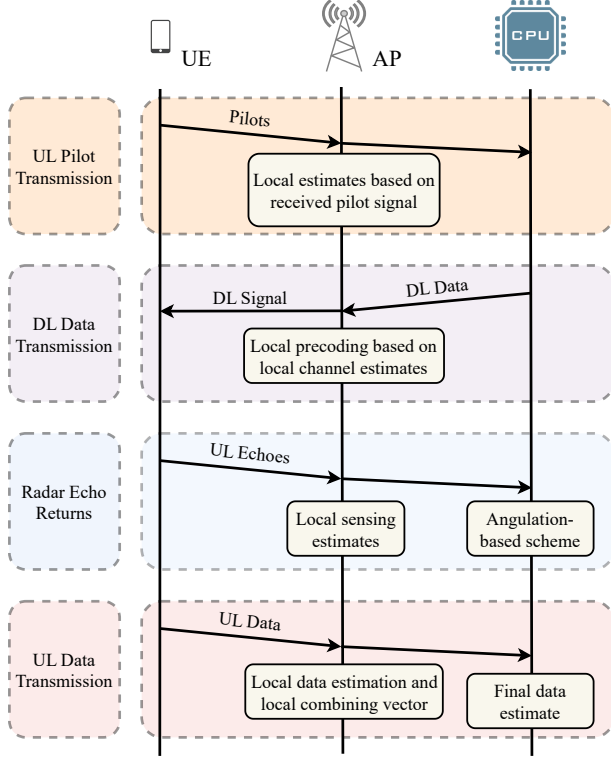


Fig. 2. Proposed distributed signaling scheme.

k -th UE is $\mathbf{h}_{kl} \in \mathbb{C}^{N \times 1}$ with collective channel from all APs as $\mathbf{h}_k = [\mathbf{h}_{k1}^T \dots \mathbf{h}_{kL}^T]^T \in \mathbb{C}^M$ with $M = NL$, (representing the total number of antennas in the coverage area). During the coherence block τ_c , \mathbf{h}_{kl} remains constant and follows a correlated Rayleigh fading distribution, $\mathbf{h}_{kl} \sim \mathcal{N}_{\mathbb{C}}(\mathbf{0}, \mathbf{R}_{kl})$ [23], where $\mathbf{R}_{kl} = \mathbb{E}[\mathbf{h}_{kl}\mathbf{h}_{kl}^H] \in \mathbb{C}^{N \times N}$ is the spatial correlation matrix, incorporating path-loss, shadowing, and spatial correlation [12]. Moreover, the channels from all APs are independently distributed, i.e., $\mathbb{E}\{\mathbf{h}_{kn}(\mathbf{h}_{kl})^H\} = \mathbf{0}$ for $l \neq n$. The collective distribution is $\mathbf{h}_k \sim \mathcal{N}_{\mathbb{C}}(\mathbf{0}, \mathbf{R}_k)$, where $\mathbf{R}_k = \text{diag}(\mathbf{R}_{k1}, \dots, \mathbf{R}_{kL}) \in \mathbb{C}^{M \times M}$ is block-diagonal spatial correlation matrix. The LSFC between the l -th AP and the k -th UE is denoted by β_{kl} , which is available at all APs and UEs. This LSFC is the normalized trace of \mathbf{R}_{kl} , given by $\beta_{kl} = \text{tr}(\mathbf{R}_{kl})/N$, and modeled as [12]

$$\beta_{kl}(\text{dB}) = \Upsilon - 10\alpha \log_{10} \left(\frac{d_{kl}}{d_{\text{ref}}} \right) + Z_{kl}, \quad (1)$$

where Υ is the path loss at reference distance d_{ref} , d_{kl} is the distance between l -th AP and k -th UE, α is the path loss exponent, and Z_{kl} is the shadowing effect, normally distributed with zero mean and standard deviation σ_{dB} . Finally, for different links of the channel vectors separate and independent realizations are obtained.

The original design of CF-mMIMO systems, where all UEs are served by all APs is impractical [24]. To ensure scalability in this case, we incorporate a set of block-diagonal matrices $\mathbf{F}_{kl} = \text{diag}(\mathbf{F}_{k1}, \dots, \mathbf{F}_{kL})$, $k = 1, \dots, K$ and $l = 1, \dots, L$, where the antenna configuration at the l -th AP for the k -th

UE is a diagonal matrix represented by $\mathbf{F}_{kl} \in \mathbb{C}^{N \times N}$. The n -th diagonal entry of \mathbf{F}_{kl} is 1 if the n -th antenna of the l -th AP is used by the k -th UE and 0 otherwise. Moreover, \mathbf{F}_{kl} determines the matrix $\mathbf{S} \in \mathbb{R}^{K \times L}$, which is defined as the association matrix. This binary matrix \mathbf{S} specifies the AP selection between UEs and APs, where for the l -th AP and the k -th UE it is defined as

$$\mathbf{S}_{kl} = \begin{cases} 1, & \text{if } \text{tr}(\mathbf{F}_{kl}) > 0 \\ 0, & \text{otherwise.} \end{cases} \quad (2)$$

where the entry $\mathbf{S}_{kl} = 1$ if the trace of \mathbf{F}_{kl} is greater than 0, indicating that the l -th AP serves the k -th UE. To improve the clarity of the mathematical descriptions, we use the notation $\mathcal{M}_k = \{l : \mathbf{S}_{kl} = 1, l \in \{1, \dots, L\}\}$ be the subset of APs serving the k -th UE, and $\mathcal{D}_l = \{k : \mathbf{S}_{kl} = 1, k \in \{1, \dots, K\}\}$ the subset of UEs served by the l -th AP.

The total coherence interval τ_c is divided into three sub-intervals: (a) uplink (UL) pilots transmission τ_p , to estimate channel between the k -th UE and the l -th AP, (b) τ_d symbols for downlink (DL) DFRC signal, through channel-matched beamforming. During this DL transmission, radar echoes are received at the APs after reflecting back from the UE, i.e., $\tau_d = \tau_{d(c)} + \tau_{u(e)}$, where $\tau_{d(c)}$ is the DL communication signal and $\tau_{u(e)}$ is the radar echo received at each AP and (c) UL data symbols τ_u .

B. Uplink Pilot Transmission and Channel Estimation

During initial access, UEs are randomly assigned pilots from a set of orthogonal signals, $\{\phi_1, \dots, \phi_{\tau_p}\}$ each with length τ_p samples, $\phi \in \mathbb{C}^{1 \times \tau_p}$. These pilot signals ensure equal power, satisfying $|\phi_t|^2 = \tau_p$, where τ_p remains constant and is independent of K . A massive access scenario is considered ($K \gg \tau_p$), leading to *pilot-sharing*. The pilot index of the k -th UE is denoted by t_k , chosen from $t_k \in \{1, 2, \dots, \tau_p\}$. Additionally, \mathcal{V}_k is a group of UEs that share the same pilots, including the k -th UE. When UEs in \mathcal{V}_k transmit pilot ϕ_{t_k} , the received signal $\mathbf{y}_{t_k l}^{\text{pilot}} \in \mathbb{C}^{N \times 1}$ at the l -th AP is as [25]

$$\mathbf{y}_{t_k l}^{\text{pilot}} = \sum_{i \in \mathcal{V}_k} \sqrt{\tau_p p_i^p} \mathbf{h}_{il} + \mathbf{n}_{t_k l}, \quad (3)$$

where p_i^p is the pilot transmit power of UE i and the thermal noise with variance σ^2 is denoted by $\mathbf{n}_{t_k l} \sim \mathcal{N}_{\mathbb{C}}(0, \sigma^2 \mathbf{I}_N)$. Moreover, (3) indicates the mutual interference that is caused by the reuse of the pilot t_k among the UEs in the set \mathcal{V}_k leading to pilot contamination [26]. The minimum mean-square error (MMSE) estimate of \mathbf{h}_{kl} for $k \in \mathcal{V}_k$ can be written as

$$\hat{\mathbf{h}}_{kl} = \sqrt{\tau_p p_k^p} \mathbf{R}_{kl} \Phi_{t_k l}^{-1} \mathbf{y}_{t_k l}^{\text{pilot}}, \quad (4)$$

where

$$\begin{aligned}
\Phi_{t_{kl}} &= \mathbb{E} \left\{ \mathbf{y}_{t_{kl}}^{\text{pilot}} \left(\mathbf{y}_{t_{kl}}^{\text{pilot}} \right)^H \right\} \\
&= \mathbb{E} \left\{ \left(\sqrt{\tau_p p_i^p} \mathbf{R}_{kl} \mathbf{h}_{kl} + \mathbf{n}_{kl} \right) \left(\sqrt{\tau_p p_i^p} \mathbf{R}_{kl} \mathbf{h}_{kl} + \mathbf{n}_{kl} \right)^H \right\} \\
&= \mathbb{E} \left\{ \sqrt{\tau_p p_i^p} \mathbf{R}_{kl} \mathbf{h}_{kl} \mathbf{h}_{kl}^H \mathbf{R}_{kl}^H \sqrt{\tau_p p_i^p} + \mathbf{n}_{kl} \mathbf{n}_{kl}^H \right\} \\
&= \tau_p p_i^p \mathbf{R}_{kl} \mathbb{E} \left\{ \mathbf{h}_{kl} \mathbf{h}_{kl}^H \right\} \mathbf{R}_{kl}^H + \mathbb{E} \left\{ \mathbf{n}_{kl} \mathbf{n}_{kl}^H \right\} = \tau_p p_i^p \mathbf{R}_{kl} \mathbf{R}_{kl}^H \\
&\quad + \sigma^2 \mathbf{I}_N = \sum_{i \in \mathcal{V}_k} \tau_p p_i^p \mathbf{R}_{il} + \sigma^2 \mathbf{I}_N. \tag{5}
\end{aligned}$$

is the correlation matrix of $\mathbf{y}_{t_{kl}}^{\text{pilot}}$, having contributions from all the UEs with same pilot sequence. The estimated channel $\hat{\mathbf{h}}_{kl}$ and the error in the estimation is $\tilde{\mathbf{h}}_{kl} = \mathbf{h}_{kl} - \hat{\mathbf{h}}_{kl}$ are independent vectors distributed as $\hat{\mathbf{h}}_{kl} \sim \mathcal{N}_{\mathbb{C}}(\mathbf{0}, \mathbf{B}_{kl})$ and $\tilde{\mathbf{h}}_{kl} \sim \mathcal{N}_{\mathbb{C}}(\mathbf{0}, \mathbf{C}_{kl})$, where

$$\mathbf{B}_{kl} = \mathbb{E} \left\{ \hat{\mathbf{h}}_{kl} \hat{\mathbf{h}}_{kl}^H \right\} = \tau_p p_k^p \mathbf{R}_{kl} \Phi_{t_{kl}}^{-1} \mathbf{R}_{kl}, \tag{6}$$

$$\mathbf{C}_{kl} = \mathbb{E} \left\{ \tilde{\mathbf{h}}_{kl} \tilde{\mathbf{h}}_{kl}^H \right\} = \mathbf{R}_{kl} - \mathbf{B}_{kl}. \tag{7}$$

Note we assume that the network has already addressed the pilot contamination issue, as this is not the focus of our work.

C. Downlink Data Transmission and Target Sensing

The DL transmission begins with APs simultaneously transmitting data and sensing the UE. Using the $\hat{\mathbf{h}}_{kl}$, the APs perform conjugate beamforming for DFRC signal transmission to the k -th UE. The transmit signal for the l -th AP in \mathcal{M}_k is

$$\mathbf{x}_l = \sqrt{p_l} \sum_{k \in \mathcal{K}} \mathbf{w}_{kl} s_k, \quad \forall l \in \mathcal{M}_k, \tag{8}$$

where p_l is the normalized signal power in the DL phase, $s_k \in \mathbb{C}$ is the data symbol for the k -th UE with $\mathbb{E}\{|s_k|^2\} = 1$, and $\mathbf{w}_{kl} \in \mathbb{C}^N$ is the beamforming vector. The normalized power budget of the l -th AP is $\mathbb{E}\{|\mathbf{x}_l|^2\} \leq p_l$, thus

$$\sum_{k \in \mathcal{K}} \mathbf{w}_{kl}^H \mathbf{w}_{kl} \leq 1, \quad \forall l \in \mathcal{M}_k. \tag{9}$$

The received superposed signal from all the APs at the UE is

$$\mathbf{y}_k^{\text{DL}} = \sum_{l=1}^L \mathbf{h}_{kl}^H \sum_{i=1}^K \mathbf{w}_{il} \mathbf{x}_l + n_k = \mathbf{h}_k^H \sum_{i=1}^K \mathbf{w}_i \mathbf{x}_l + n_k, \tag{10}$$

where $\mathbf{w}_k = [\mathbf{w}_{k1}^T \dots \mathbf{w}_{kL}^T]^T \in \mathbb{C}^M$ is the collective precoding vector, and $n_k \sim \mathcal{N}_{\mathbb{C}}(0, \sigma^2)$ is the receiver noise. The most popular choice is maximum ratio (MR) precoding with [8]

$$\mathbf{w}_{il} = \sqrt{p_i} \frac{\hat{\mathbf{h}}_{il}}{\sqrt{\mathbb{E}\{|\hat{\mathbf{h}}_{il}|^2\}}}, \tag{11}$$

where $p_i \geq 0$ is the transmit power allocated to the UE i . **Note:** In beamforming towards the UE, we start with a coarse location, \mathbf{u}_k , assuming the UE is within the transmission's beam width. For sensing, however, centimeter-level accuracy is often required [27]. Therefore, we refine the UEs position later in Section IV-B.

D. Uplink Radar Echoes Reception

The APs which transmit DL DFRC signal, are considered to receive radar echoes reflected from the UE and also unwanted signals from clutter, which is considered as interference for sensing. The goal is to establish LoS links to eliminate sensing interference from clutter, as further explained in this paper. The echo received at the l -th AP is

$$\begin{aligned}
\mathbf{y}_l^{\text{echo}} &= \sum_{k=1}^N \underbrace{\xi_{kl} \sqrt{\zeta_{kl}} \mathbf{a}(\phi_{0,l}, \theta_{0,l}) \mathbf{a}^T(\varphi_{0,k}, \vartheta_{0,k}) \mathbf{x}_l}_{\text{desired reflection from the UE}} \\
&\quad + \sum_{k=1}^N \underbrace{\mathbf{H}_{kl} \mathbf{x}_k}_{\text{undesired echoes from clutter}} + \mathbf{n}_l, \tag{12}
\end{aligned}$$

where $\mathbf{n}_l \sim \mathcal{CN}(\mathbf{0}, \sigma^2 \mathbf{I}_N)$ is the receiver noise, ζ_{kl} is the channel gain including the path loss from the l -th AP and the k -th UE, while ξ_{kl} is the normalized RCS of the UE for the respective path. Moreover, the respective array response vector is $\mathbf{a}(\phi, \theta) = [1 \ e^{j\pi \sin(\phi) \cos(\theta)} \dots e^{j(N-1)\pi \sin(\phi) \cos(\theta)}]^T$, where ϕ and θ are the azimuth and elevation angles from the AP to the UE respectively [23], while \mathbf{H}_{kl} is the target-free channel matrix between the l -th AP and the k -th UE.

E. Uplink Data Transmission

The received UL signal $\mathbf{y}_l^{\text{UL}} \in \mathbb{C}^N$ at the l -th AP is

$$\mathbf{y}_l^{\text{UL}} = \sum_{i=1}^K \mathbf{h}_{il} s_i + \mathbf{n}_l, \tag{13}$$

where $s_i \sim \mathcal{N}_{\mathbb{C}}(0, p_i)$ represents the signal transmitted by the UE i with power p_i , and $\mathbf{n}_l \sim \mathcal{N}_{\mathbb{C}}(0, \sigma^2 \mathbf{I}_N)$ is the noise. Each AP estimates the data locally before forwarding it to the CPU for final decoding, as illustrated in Fig. 2. The combining vector used by the l -th AP for the k -th UE is denoted as $\mathbf{a}_{kl} \in \mathbb{C}^N$, where $k \in \mathcal{D}_l$. The local estimate of s_k can then be expressed as

$$\begin{aligned}
\tilde{s}_{kl} &= \mathbf{a}_{kl}^H \mathbf{D}_{kl} \mathbf{y}_l^{\text{UL}} \\
&= \mathbf{a}_{kl}^H \mathbf{D}_{kl} \mathbf{h}_{kl} s_k + \mathbf{a}_{kl}^H \mathbf{D}_{kl} \sum_{i=1, i \neq k}^K \mathbf{h}_{il} s_i + \mathbf{a}_{kl}^H \mathbf{D}_{kl} \mathbf{n}_l. \tag{14}
\end{aligned}$$

Any combining vector can be utilized in the above expression. MR combining, with $\mathbf{a}_{kl}^{\text{MR}} = \hat{\mathbf{h}}_{kl}$, was employed in [28]. More recently, [8] proposed the use of local partial MMSE combining

$$\mathbf{a}_{kl}^{\text{LP-MMSE}} = p_k \left(\sum_{i \in \mathcal{D}_l} p_i \left(\hat{\mathbf{h}}_{il} \hat{\mathbf{h}}_{il}^H + \mathbf{C}_{il} \right) + \sigma^2 \mathbf{I}_N \right)^{-1} \hat{\mathbf{h}}_{kl}. \tag{15}$$

The local estimates $\{\tilde{s}_{kl}\}$ are subsequently transmitted to the CPU, where they are linearly combined with weights $\{w_{kl}\}$ to produce $\hat{s}_k = \sum_{l=1}^L w_{kl}^* \tilde{s}_{kl}$, which is then utilized for decoding s_k . Using (14), the final estimate of s_k is derived as follows

$$\hat{s}_k = \mathbf{a}_k^H \mathbf{W}_k^H \mathbf{D}_k \mathbf{h}_k s_k + \sum_{i=1, i \neq k}^K \mathbf{a}_k^H \mathbf{W}_k^H \mathbf{D}_k \mathbf{h}_i s_i + \mathbf{a}_k^H \mathbf{W}_k^H \mathbf{D}_k \mathbf{n}, \tag{16}$$

where $\mathbf{W}_k = \text{diag}(w_{k1} \mathbf{I}_N, \dots, w_{kL} \mathbf{I}_N) \in \mathbb{C}^{(LN) \times (LN)}$.

$$\text{SINR}_k = \frac{p_k |\mathbb{E} \{ \mathbf{a}_k^H \mathbf{W}_k^H \mathbf{D}_k \mathbf{h}_k \} |^2}{\sum_{i=1}^K p_i \mathbb{E} \{ |\mathbf{a}_k^H \mathbf{W}_k^H \mathbf{D}_k \mathbf{h}_i|^2 \} - p_k |\mathbb{E} \{ \mathbf{a}_k^H \mathbf{W}_k^H \mathbf{D}_k \mathbf{h}_k \} |^2 + \sigma^2 \mathbb{E} \{ \|\mathbf{D}_k \mathbf{W}_k^H \mathbf{a}_k\|^2 \}}$$

$$\text{SINR}_k = \frac{p_k |\mathbf{w}_k^H \mathbf{v}_k|^2}{\mathbf{w}_k^H \left(\sum_{i=1}^K p_i \mathbf{\Lambda}_{ki}^{(1)} - p_k \mathbf{v}_k \mathbf{v}_k^H + \sigma^2 \mathbf{\Lambda}_k^{(2)} \right) \mathbf{w}_k}, \quad (18)$$

III. PROBLEM FORMULATION

In this section, we first explain the concepts of SE and SCNR, on which our optimization problems are based. Following this, we present the optimization problems that ensure effective JRC UA in CF-mMIMO systems.

A. Achievable Spectral Efficiency

The achievable SE for the k -th UE in CF-mMIMO network is expressed as [8]

$$\text{SE}_k = \left(1 - \frac{\tau_p}{\tau_c} \right) \log_2(1 + \text{SINR}_k), \quad (17)$$

where the effective signal-to-interference-plus-noise ratio (SINR) of the k -th UE is denoted as SINR_k . In (18),

$$\mathbf{w}_k = [w_{k1}, \dots, w_{kL}]^T, \quad (19a)$$

$$\mathbf{v}_k = [\mathbb{E} \{ \mathbf{a}_{k1}^H \mathbf{D}_{k1} \mathbf{h}_{k1} \}, \dots, \mathbb{E} \{ \mathbf{a}_{kL}^H \mathbf{D}_{kL} \mathbf{h}_{kL} \}]^T, \quad (19b)$$

$$\mathbf{\Lambda}_{ki}^{(1)} = [\mathbb{E} \{ \mathbf{a}_{kl}^H \mathbf{D}_{kl} \mathbf{h}_{il} \mathbf{h}_{ij}^H \mathbf{D}_{kj} \mathbf{a}_{kj} \} : l, j = 1, \dots, L], \quad (19c)$$

$$\mathbf{\Lambda}_k^{(2)} = \text{diag} \left(\mathbb{E} \{ \|\mathbf{D}_{k1} \mathbf{a}_{k1}\|^2 \}, \dots, \mathbb{E} \{ \|\mathbf{D}_{kL} \mathbf{a}_{kL}\|^2 \} \right), \quad (19d)$$

B. Signal-Clutter plus Noise Ratio

For a specified range resolution cell of the AP used for sensing, the SCNR is $\frac{P_{ue}}{P_c + P_n}$, where P_{ue} and P_c are the powers of the UE and clutter backscatter, respectively, and P_n is the noise power. We consider a scenario with multiple discrete scatterers making up the clutter \mathbf{c} around a specific UE, these scatterers' positions are modeled as a 2D Poisson point process (PPP) (Γ') [29], with a uniform distribution. The RCS of these scatterers follows a standard Swerling cross-section model as described in [30]. The closest distance between the clutter scatterers and the AP is R , which is within the radar's maximum unambiguous range. The RCS of each scatterer (v_c) contributing to the clutter follows the distribution

$$P(v_c) = \frac{1}{v_{c,avg}} \exp \left(-\frac{v_c}{v_{c,avg}} \right), \quad (20)$$

where $v_{c,avg}$ is the average clutter cross-section. For each realization of the PPP, the total received clutter power is [30]

$$\mathbf{C} = \sum_{c \in \Gamma'} \frac{ZG(\theta_c)v_c g_c}{\mathbf{r}_c^{2q}}, \quad (21)$$

where Z is a constant and defined as $Z = \frac{p_l \lambda^2}{(4\pi)^3}$, $G(\theta_c) = G_{tx}(\theta_c)G_{rx}(\theta_c)$ ($G_{tx}(\theta)$ and $G_{rx}(\theta)$ being the directional transmit and receive antenna gains, respectively), g_c is a random variable modeling the fading between clutter returns, and q is path loss exponent. The position of each scatterer \mathbf{c}

is given in polar coordinates as $\bar{\mathbf{r}}_c = (\mathbf{r}_c, \theta_c)$, with azimuth θ_c uniformly distributed in $[0, 2\pi)$ and range \mathbf{r}_c in $(R, \infty]$. For a UE cross-section of v_t , the received signal at the AP is $\mathbf{S}_s = \frac{ZG(\theta_t)v_t}{\mathbf{r}_t^{2q}}$, where $G(\theta_t) = G_{tx}(\theta_t)G_{rx}(\theta_t)$. We assume a Swerling-1 RCS fluctuation for the UE.

$$P(v_t) = \frac{1}{v_{t,avg}} \exp \left(-\frac{v_t}{v_{t,avg}} \right), \quad (22)$$

where $v_{t,avg}$ represents the average UE cross-section. Under LoS conditions, the minimum SCNR occurs when $\mathbf{r}_t = R$. Assuming the AP tracks the UE within its main beam, such that $G(\theta_t) = 1$ therefore, the average SCNR for a given R is

$$\mathbb{E} [\text{SCNR}(R)] = \mathbb{E}_{v_t, v_c, g_c, \Gamma'} \left[\frac{\frac{Zv_t}{R^{2q}}}{n_l + \sum_{c \in \Gamma} \frac{ZG(\theta_c)v_c g_c}{\mathbf{r}_c^{2q}}} \right]. \quad (23)$$

In the context of the proposed JRC CF-mMIMO scenario, mitigating clutter is crucial for accurate UE detection/tracking and AP association. One important metric in understanding the impact of clutter in front of a specific UE and AP view angle, is the P_{dc} . This is defined as the probability that the average SCNR at a distance r is greater than or equal to a predefined threshold γ

$$P_{dc}(r) \triangleq \mathbb{P}(\text{SCNR}(r) \geq \gamma). \quad (24)$$

In the following theorems, we will delve deeper into the mathematical analysis to characterize P_{dc} in both LoS and NLoS conditions, highlighting the significance of the proposed UA. These analyses will provide better insight into the clutter surrounding a UE and underscore the importance of considering clutter factor when selecting APs.

Theorem 1. *The P_{dc} for the UE located at LoS distance R from a AP without any clutter, such that $G(\theta_t) = 1$ is as*

$$P_{dc}(R) = I(R) \exp \left(\frac{-\gamma n_l R^{2q}}{Z v_{t,avg}} \right), \quad (25)$$

where $I(R) = \exp \left(-\rho \int_0^{2\pi} \int_R^{R+\Delta R} \frac{\nu(R)G(\theta_c)r_c}{\nu(R)G(\theta_c)+r_c^{2q}} dr_c d\theta_c \right)$, and $\nu(R) = \frac{\gamma R^{2q} v_{c,avg}}{v_{t,avg}}$, From (25) we have,

$$P_{dc}(R) = \mathbb{P} \left[v_t > \frac{\gamma n_l R^{2q}}{Z} + \gamma R^{2q} \sum_{c \in \Gamma} \frac{G(\theta_c)v_c g_c}{\mathbf{r}_c^{2q}} \right] \quad (26a)$$

$$= \mathbb{E}_{v_c, g_c, \Gamma'} \left[\exp \left(\frac{-\gamma n_l R^{2q}}{Z v_{t,avg}} - \frac{\gamma R^{2q}}{v_{t,avg}} \sum_{c \in \Gamma} \frac{G(\theta_c)v_c g_c}{\mathbf{r}_c^{2q}} \right) \right] \quad (26b)$$

$$= \exp \left(\frac{-\gamma n_l R^{2q}}{Z v_{t,avg}} \right) \mathbb{E}_{v_c, g_c, \Gamma'} \left[\prod_{c \in \Gamma} \exp \left(\frac{-\gamma R^{2q} G(\theta_c)v_c g_c}{v_{t,avg} \mathbf{r}_c^{2q}} \right) \right], \quad (26c)$$

where (26a) assumes UE cross-section follows (22), while (26b) results from taking the expectation, considering clutter scatterers, cross-sections, spatial distribution, and mutual interference. Using the property that exponentials of sums equal products of exponential functions yields (26c). Additionally, evaluating the expectation using the probability generating functional of the point process Γ gives [29]

$$\mathbb{E}_{v_c, g_c, \Gamma'} \left[\prod_{c \in \Gamma'} \exp \left(\frac{-\gamma R^{2q} G(\theta_c) v_c g_c}{v_{\text{avg}} r_c^{2q}} \right) \right] = \exp \left(-\varrho \int_{\mathbb{R}^2} \left(1 - \mathbb{E}_{v_c, g_c} \left[\exp \left(\frac{-\gamma R^{2q} G(\theta_c) v_c g_c}{v_{\text{avg}} r_c^{2q}} \right) \right] \right) d(\vec{r}_c) \right). \quad (27)$$

The expectation inside the integral is taken for the interference g_c and the scatterer cross-section v_c . Under the worst scenario, $g_c = 1$ (indicating that signals from all scatterers add constructively, resulting in the maximum clutter returns), and assuming the scatterer cross-section follows (20), we derive

$$\begin{aligned} \mathbb{E}_{v_c, g_c} \left[\exp \left(\frac{-\gamma R^{2q} G(\theta_c) v_c g_c}{v_{\text{avg}} r_c^{2q}} \right) \right] &= \frac{1}{1 + \frac{\gamma R^{2q} G(\theta_c) v_{\text{cavg}}}{v_{\text{avg}} r_c^{2q}}} \\ &= \frac{1}{1 + \frac{\nu(R)G(\theta_c)}{r_c^{2q}}}, \end{aligned} \quad (28)$$

where $\nu(R) = \frac{\gamma R^{2q} v_{\text{cavg}}}{v_{\text{avg}}}$. Now, substituting this into (27)

$$\begin{aligned} \mathbb{E}_{v_c, g_c, \Gamma'} \left[\prod_{c \in \Gamma'} \exp \left(\frac{-\gamma R^{2q} G(\theta_c) v_c g_c}{v_{\text{avg}} r_c^{2q}} \right) \right] &= \exp \left(-\varrho \int_{\mathbb{R}^2} \left(1 - \frac{1}{1 + \frac{\nu(R)G(\theta_c)}{r_c^{2q}}} \right) d(\vec{r}_c) \right), \end{aligned} \quad (29)$$

Simplifying inside the exponential

$$1 - \frac{1}{1 + \frac{\nu(R)G(\theta_c)}{r_c^{2q}}} = \frac{\frac{\nu(R)G(\theta_c)}{r_c^{2q}}}{1 + \frac{\nu(R)G(\theta_c)}{r_c^{2q}}} = \frac{\nu(R)G(\theta_c)r_c^{2q}}{\nu(R)G(\theta_c) + r_c^{2q}}, \quad (30)$$

So the integral becomes

$$\exp \left(-\varrho \int_0^{R+\Delta R} \int_R \frac{\nu(R)G(\theta_c)r_c}{\nu(R)G(\theta_c) + r_c^{2q}} dr_c d\theta_c \right), \quad (31)$$

where (31) is the $I(R)$, which was defined in **Theorem 1**. Note that in this scenario clutter from scatterers that lie within the same range resolution cell of the UE is considered (R and $R + \Delta R$, where $\Delta R = c/2BW$, the range resolution is estimated from the bandwidth, BW of the radar).

Furthermore, when considering NLoS scenario where clutter obstructs the view angle between the AP and the UE, the radar signal to the UE and its return to the AP undergo exponential decay due to propagation through the material of the clutter scatterers. The UE can be detected when the SCNR at the range cell occupied by the UE meets or exceeds the predefined threshold. The clutter consists of a set of discrete scatterers, whose positions ($\vec{r}_c = \mathbf{r}_c, \theta_c$) follow a PPP Γ defined in \mathbb{R}^2 , with UE located at $\vec{r}_t = (r_t, \theta_t)$. The attenuation factor due

to the material properties of the scatterer is assumed to be $\alpha(\lambda_c)$. Since the region between the radar and the target is partially covered with clutter, the attenuation α is factored with ϱv_0 where ϱ is the intensity measure of the PPP while v_0 is the average physical area occupied by the scatterers. Then the received signal from the UE is $\mathbf{S} = \frac{ZG(\theta_t)v_t e^{-2\alpha' r_t}}{r_t^{2q}}$. Similarly, the clutter returns are

$$\mathbf{C} = \sum_{c \in \Gamma} \frac{ZG(\theta_c) e^{-2\alpha' r_c} v_c g_c}{r_c^{2q}}. \quad (32)$$

Theorem 2. The P_{dc} of a UE at NLoS distance r_t from the AP within the field of view such that $G(\theta_t) = 1$ is

$$P_{DC}(r_t) = J(r_t) \exp \left(\frac{-\gamma n_l r_t^{2q} e^{2\alpha' r_t}}{Z v_{\text{avg}}} \right) \quad (33)$$

where

$$J(r_t) = \exp \left(-\varrho \int_0^{2\pi} \int_{r_t}^{r_t+\Delta R} \frac{\nu'(r)G(\theta_c)r_c}{\nu'(r)G(\theta_c) + r_c^{2q} e^{2\alpha' r_c}} dr_c d\theta_c \right), \quad (34)$$

and

$$\nu'(r_t) = \frac{\gamma r_t^{2q} e^{2\alpha' r_t} v_{\text{cavg}}}{v_{\text{avg}}}. \quad (35)$$

From the definition of P_{dc} , we have (*Proof*. See Appendix),

$$\begin{aligned} P_{DC}(r_t) &= \mathbb{P}[\text{SCNR}(r_t) > \gamma] = \\ &= \mathbb{P} \left[\frac{\frac{Z v_t}{r_t^{2q}} e^{-2\alpha' r_t}}{n_l + \sum_{c \in \Gamma} \frac{ZG(\theta_c)v_c g_c}{r_c^{2q}}} e^{-2\alpha' r_c} > \gamma \right]. \end{aligned} \quad (36)$$

C. Optimization Problems

When the k -th UE accesses the network, it selects its serving APs from \mathcal{M}_k . This selection is limited because each AP can only accommodate up to τ_p UEs. Ensuring scalability in CF-mMIMO systems hinges on two crucial assumptions, limiting each AP to τ_p associated UEs and ensuring all N antennas of APs serve the UEs, ($|\mathcal{D}_l| \leq \tau_p$)

$$\mathbf{D}_{kl} = \begin{cases} \mathbf{I}_N & \text{if } k \in \mathcal{D}_l \\ \mathbf{0}_N & \text{otherwise} \end{cases}, \text{ for } l = 1, \dots, L. \quad (37)$$

The UA problem on a given pilot assignment is

$$\mathbf{P1} : \max_{\mathbf{S}^{(j)}} \sum_{k=1}^K \text{SE}_k^{(j)} \quad \forall j = 1, \dots, J \quad (38a)$$

$$\text{s.t. } |\mathcal{M}_l^{(j)}| \leq \tau_p \quad \forall j = 1, \dots, J \quad \forall l = 1, \dots, L \quad (38b)$$

$$|\mathcal{V}_k^{(j)}| \geq 2 \quad \forall j = 1, \dots, J \quad \forall k = 1, \dots, K \quad (38c)$$

where $\mathbf{S}^{(j)}$ is the association matrix and $\text{SE}_k^{(j)}$ is the k -th UE SE under the j -th combination, resulting in $J = \binom{K}{\tau_p}^L$, where $\binom{K}{\tau_p}$ denotes combinations of τ_p UEs from K for a single AP. The constraint (38b) ensures scalability, limiting number of UEs each AP can serve. While (38c) ensures each UE is served by at least two APs, ensuring coverage and reliability. This also facilitates angulation-based clutter detection (Section

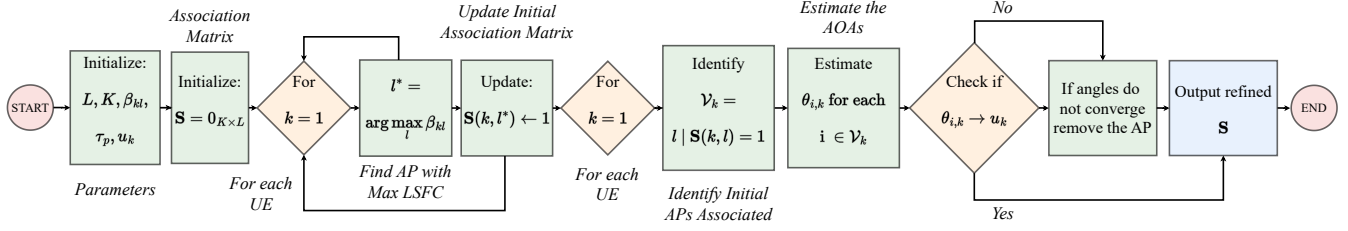


Fig. 3. Flowchart of the proposed scheme.

Algorithm 1 Initial Phase UA

- 1: **Input:** $L, K, \{\beta_{kl}\}, \tau_p$
- 2: **Output:** \mathbf{S}
- 3: Initialize: $\mathbf{S} = 0_{K \times L}$
- 4: **for** $k = 1 : K$ **do**
- 5: $l^* = \arg \max_l \beta_{kl}$
- 6: $\mathbf{S}(k, l^*) \leftarrow 1$
- 7: **end for**
- 8: **for** $l = 1 : L$ **do**
- 9: $\mathcal{L}_{UE,l} = \text{argsort}(\beta_{kl}, \text{descending})$
- 10: $\mathcal{B}_l = \text{first}(\tau_p - |\mathcal{M}_l|)$ elements of $\mathcal{L}_{UE,l}$
- 11: **for each** k in \mathcal{B}_l **do**
- 12: $\mathbf{S}(k, l) \leftarrow 1$
- 13: **end for**
- 14: **end for**
- 15: **for** $l = 1 : L$ **do**
- 16: $\mathcal{L}_{R,l} = \text{find repeated UEs in } \mathcal{M}_l$
- 17: **while** $|\mathcal{L}_{R,l}| > 0$ **do**
- 18: $k^* = (\tau_p - |\mathcal{M}_l| + i)$ th element of $\mathcal{L}_{UE,l}$, where $i = 1, 2, \dots, |\mathcal{L}_{R,l}|$
- 19: $\mathbf{S}(k^*, l) \leftarrow 1$
- 20: $\mathcal{L}_{R,l} = \text{update repeated UEs in } \mathcal{M}_l$
- 21: **end while**
- 22: **end for**

Algorithm 2 Second Phase UA

- 1: **Input:** $L, K, \{\theta_{i,k}\}, \tau_p, \mathbf{u}_k$, Initial association matrix \mathbf{S} from Algorithm 1
- 2: **Output:** Refined association matrix \mathbf{S}
- 3: **for** $k = 1 : K$ **do**
- 4: $\mathcal{V}_k = \{l \mid \mathbf{S}(k, l) = 1\}$ {Initial APs associated with UE k }
- 5: **for** $i \in \mathcal{V}_k$ **do**
- 6: Compute $\theta_{i,k}$ {Angle from AP i to UE k }
- 7: **end for**
- 8: Check if angles converge at the estimated UE location
- 9: **if** angles do not converge **then**
- 10: Remove i from \mathcal{V}_k
- 11: Update $\mathbf{S}(k, i) \leftarrow 0$
- 12: **end if**
- 13: **end for**
- 14: **for** $k = 1 : K$ **do**
- 15: $\mathcal{V}_k = \{l \mid \mathbf{S}(k, l) = 1\}$
- 16: **if** $|\mathcal{V}_k| < 2$ **then**
- 17: $l^* = \arg \min_l \theta_{i,k}$ where $l \notin \mathcal{V}_k$
- 18: $\mathbf{S}(k, l^*) \leftarrow 1$
- 19: **end if**
- 20: **end for**
- 21: **return** \mathbf{S}

IV-B), enhancing sensing accuracy. **P1** is non-deterministic Polynomial time (NP)-hard due to its combinatorial nature, but optimal solutions can be explored using methods like exhaustive search across all J combinations. However, the practical considerations of system parameters K, τ_p , and L affect the computational complexity.

To solve this optimization, Algorithm 1 initializes \mathbf{S} to zero, having no initial associations. The algorithm comprises three parts: UE preference-based association, AP preference, and handling repeated associations. For UE preference, each UE selects the AP l^* with the strongest LSFC, updating \mathbf{S} . AP preference involves each AP identifying a subset of UEs based on LSFC, selecting up to $(\tau_p - |\mathcal{M}_l|)$ UEs. Handling repeated associations ensures each UE is served by at least two APs without exceeding the AP capacity. The final \mathbf{S} matrix guarantees each UE is served by at least two APs, without surpassing τ_p , and efficiently resolves the NP-hard problem.

To achieve optimal JRC UA, it is crucial to consider the sensing aspects beyond SE of the communication system. For sensing, the echoes must be received solely from the

UE, avoiding clutter. Thus, the association must ensure that each UE is served by APs providing the highest SCNR while maintaining LoS conditions through angle-of-arrival (AOA) convergence. This convergence is achieved by exploiting AOA based positioning [31], [32], which identifies the APs that have clutter in their view angle with a UE. A heuristic-based solution is proposed here to maximize the minimum SCNR while ensuring at least two APs serve each UE with LoS conditions. This approach is executed after forming the initial LSFC-based cluster. The cluster is then refined by eliminating APs unsuitable for sensing. The formulation is

$$\begin{aligned}
 \mathbf{P2} : & \max_{\mathbf{S}} \min_{k \in \{1, \dots, K\}} \{\text{SCNR}_k\} \\
 \text{s.t.} & \quad |\mathcal{V}_k| \geq 2, \quad \forall k = 1, \dots, K \\
 & \quad \theta_{i,k} \text{ ensures LoS conditions, } \forall i \in \mathcal{V}_k \\
 & \quad \theta_{i,k} \text{ from APs to UE converge at } u_k, \forall i \in \mathcal{V}_k
 \end{aligned} \tag{39}$$

To solve this optimization problem, the detailed pseudo-code is provided in Algorithm 2. This algorithm begins with the initial association matrix \mathbf{S} from Algorithm 1, which is

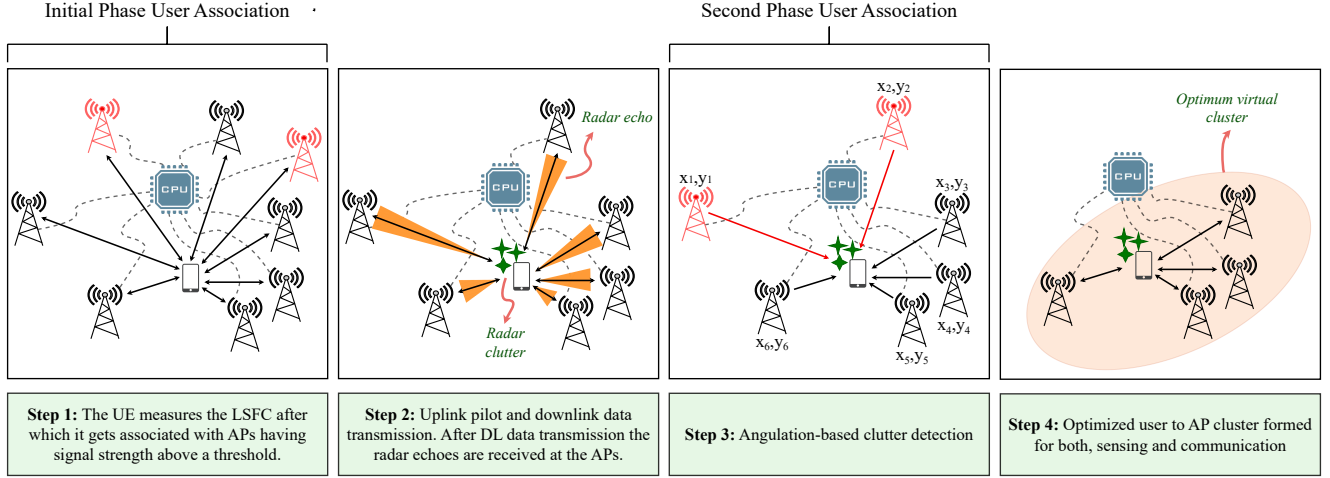


Fig. 4. Block diagram of the proposed UA technique.

filled based on the initial association via LSFC. In the second step, the angulation-based scheme is applied to the same APs that were associated in the first step. This ensures that the association is not restarted but refined, by removing those APs that are not suitable for sensing. The method ensures that each UE is served by APs that provide the highest SCNR which is detailed in Section IV-B. Moreover, both **P1** and **P2** are summarized in a flowchart as illustrated in Fig. 3.

IV. PROPOSED USER ASSOCIATION

Despite the potential benefits of CF-mMIMO, effective UA is essential to optimize system performance. Traditional UA methods may not fully leverage CF-mMIMO capabilities in a JRC scenario, as they focus solely on communication metrics such as signal strength or SINR. This problem now involves dynamically assigning a UE to APs based on communication and sensing considerations. The key challenge is to develop a scheme that effectively balances communication performance and sensing accuracy. Our proposed UA technique, shown in Fig. 4, addresses this issue.

A. Initial Phase for User Association

For each UE-AP pair, the specific UE first measures the β_{kl} for all nearby APs. This is done using the primary and secondary synchronization signals, a standard feature in cellular networks, and is broadcasted periodically to facilitate such measurements [8]. By measuring β_{kl} , the UE selects the highest values and associates with those APs. Let $\mathcal{L}_{AP,k}$ denote the set of APs available for the k -th UE. The UE aims to find the l -th AP that maximizes the value β_{kj} , given by $l = \arg \max_{j \in \mathcal{L}_{AP,k}} \beta_{kl}$, where the index j ranges over $\mathcal{L}_{AP,k}$, representing the available APs. Moreover, we can rewrite \mathcal{M}_k which is the subset of selected APs, $\mathcal{M}_k = \{j \in \mathcal{L}_{AP,k} : \beta_{kj} \geq \xi\}$, where ξ is a threshold for minimum acceptable β_{kl} . Finally, the UE associates with the APs in \mathcal{M}_k ensuring the criteria for optimal communication performance.

B. Second Phase for User Association:

Once the initial phase APs are selected, the next step follows by the UL pilots transmission and APs transmitting DFRC

beam. When the DFRC beam is directed towards the UE, reflected radar echoes are received at each AP. These echoes help estimate the UEs parameters such as its range, velocity, and angular estimates, as described in [33]. In this work, the AOA estimates from the DFRC echo received by the APs are exploited to detect clutter around the desired target, resulting in the exclusion of APs with clutter in their view angles.

In Cartesian coordinate system let $\mathbf{u}'_k = [x \ y]^T$ be the real position of the UE and $\mathbf{p}_l = [x_l \ y_l]^T$, ($l = 1, \dots, n$) the position of the l -th AP. Without loss of generality, the position of one of the APs is considered at origin i.e., $\mathbf{p}_1 = [x_1 \ y_1]^T \equiv [0 \ 0]^T$. Moreover, α_i is the AOA estimated from echo at l -th AP. Let L_{1d} be the distance between AP₁ and AP_d, ($d = 2, \dots, n$), as illustrated in Fig. 5. Since the network already knows the locations of each AP, using the abscissa and the ordinate [34], [35] and combining the estimated AOAs, the position where the AOA bearings intersect

$$\text{at } \mathbf{u}'_k \text{ is } \begin{bmatrix} x \\ y \end{bmatrix} = \begin{bmatrix} \frac{\cos \alpha_1 \sin \alpha_n}{\sin(\alpha_1 + \alpha_n)} L_{1d} \\ \frac{\sin \alpha_1 \sin \alpha_n}{\sin(\alpha_1 + \alpha_n)} L_{1d} \end{bmatrix}, \text{ [31]. Combining all}$$

these equations leads to $\mathbf{G}\mathbf{u}'_k = \mathbf{b}$. Since it is linearized, the least square estimator provides the intersection estimate, $\mathbf{u}'_{k(\text{LS})} = (\mathbf{G}^T \mathbf{G})^{-1} \mathbf{G}^T \mathbf{b}$, where

$$\mathbf{u}'_k = \begin{bmatrix} x \\ y \end{bmatrix}, \quad \mathbf{G} = \begin{bmatrix} 1 & 0 \\ 0 & 1 \\ 1 & 0 \\ 0 & 1 \\ \vdots & \vdots \\ 1 & 0 \\ 0 & 1 \end{bmatrix}, \quad \mathbf{b} = \begin{bmatrix} \frac{\cos(\alpha_1) \sin(\alpha_2)}{\sin(\alpha_1 + \alpha_2)} L_{12} \\ \frac{\sin(\alpha_1) \sin(\alpha_2)}{\sin(\alpha_1 + \alpha_2)} L_{12} \\ \vdots \\ \frac{\cos(\alpha_1) \sin(\alpha_n)}{\sin(\alpha_1 + \alpha_n)} L_{1d} \\ \frac{\sin(\alpha_1) \sin(\alpha_n)}{\sin(\alpha_1 + \alpha_n)} L_{1d} \end{bmatrix}. \quad (40)$$

In case when there is clutter in front of a specific AP view angle with the UE, the AOA will be corrupted and will have wrong estimates. Therefore the error measurements will be $u_e \alpha_1$ and $u_e \alpha_2$ instead of α_1 and α_2 respectively as shown in Fig. 5 (b). Moreover, the term u_{e_s} in the abscissa and the ordinate is expressed as $u_{e_s} = \left. \frac{\partial(x,y)}{\partial(\alpha_1, \alpha_2)} \right|_{u_e \alpha_1 u_e \alpha_2}$. Thus, the derivatives of x and y with respect to their AOAs are

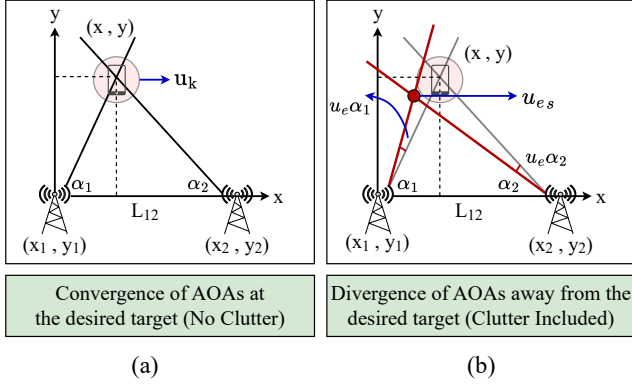


Fig. 5. Angulation-based clutter detection technique.

$$\begin{bmatrix} \frac{\partial x}{\partial \alpha_1} & \frac{\partial x}{\partial \alpha_2} \\ \frac{\partial y}{\partial \alpha_1} & \frac{\partial y}{\partial \alpha_2} \end{bmatrix} = \begin{bmatrix} -\sin \alpha_2 \cos \alpha_2 & \sin \alpha_1 \cos \alpha_1 \\ \sin^2(\alpha_1 + \alpha_2) & \sin^2(\alpha_1 + \alpha_2) \\ \sin^2 \alpha_2 & \sin^2 \alpha_1 \\ \sin^2(\alpha_1 + \alpha_2) & \sin^2(\alpha_1 + \alpha_2) \end{bmatrix} L_{12},$$

$$\left| \frac{\partial(x, y)}{\partial(\alpha_1, \alpha_2)} \right| = \left| \frac{\sin \alpha_1 \sin \alpha_2}{\sin^3(\alpha_1 + \alpha_2)} \right| L_{12}^2, \text{ replacing this into the}$$

u_{e_s} equation yields $u_{e_s} = L_{12}^2 \left| \frac{\sin \alpha_1 \sin \alpha_2}{\sin^3(\alpha_1 + \alpha_2)} \right| d\alpha_1 d\alpha_2$. In this context, the point u_{e_s} represents the intersection of the AOAs from two APs, which were inaccurately estimated due to clutter obstructing the view between the AP and the UE. The requirement of at least two APs connected to a UE allows for the intersection of their angles. If the angles intersect around the coarse position \mathbf{u}_k^c of the UE, it indicates no clutter in front of this specific AP. Suppose they intersect elsewhere, as illustrated in Fig. 5 (b), in that case, it suggests that the AOA estimate from the radar echo was affected by clutter, causing the incorrect AOA estimation to deviate from \mathbf{u}_k^c . This method allows us to identify any AP obstructed by clutter, enabling its removal from the AP cluster. By doing so, the echoes received are solely from the target, eliminating interference from surrounding clutter. This approach increases LoS links, thereby enhancing the SCNR and overall sensing performance.

C. Final Optimized Cluster

Once the APs designated to serve a specific UE are determined by following the steps outlined in Section IV-A and IV-B, as illustrated in Fig. 4, these selected APs will continuously sense and communicate with the UE. For the communication process, conventional CF-mMIMO transmission, reception, and decoding techniques are employed, as detailed in [8], [10], and [36], which are also discussed in Section II. Meanwhile, we use the following optimal sensing detector to track the UE constantly. The reflected echo signals from the UE to all the APs are sent to the CPU for combined detection. Using all these received signals, the detection leads to the following binary hypothesis problem [37]

$$\begin{cases} H_0 : \mathbf{y} = \mathbf{c} + \mathbf{n} \\ H_1 : \mathbf{y} = \mathbf{x} + \mathbf{c} + \mathbf{n} \end{cases} \quad (41)$$

where $\mathbf{y}, \mathbf{x}, \mathbf{c}$, and \mathbf{n} are defined by column-wise stacking of $\mathbf{y}_l, \mathbf{x}_l, \mathbf{c}_l$, and \mathbf{n}_l for $l = 1, 2, \dots, N$. More precisely, $\mathbf{y} \triangleq [\mathbf{y}_1^T \dots \mathbf{y}_N^T]^T$, $\mathbf{x} \triangleq [\mathbf{x}_1^T \dots \mathbf{x}_N^T]^T$, $\mathbf{c} \triangleq [\mathbf{c}_1^T \dots \mathbf{c}_N^T]^T$,

and $\mathbf{n} \triangleq [\mathbf{n}_1^T \dots \mathbf{n}_N^T]^T$. Let $\{\mathbf{N}_l\}$ denote the covariance matrices of Gaussian random vectors $\{\mathbf{n}_l\}$. Further let \mathbf{X}, \mathbf{C} , and \mathbf{N} represent the covariance matrices of \mathbf{x}, \mathbf{c} , and \mathbf{n} respectively. Using the assumptions mentioned earlier we have $\mathbf{X} = \text{blkDiag}(\sigma_1^2 \mathbf{a}\mathbf{a}^H, \sigma_2^2 \mathbf{a}\mathbf{a}^H, \dots, \sigma_N^2 \mathbf{a}\mathbf{a}^H)$, $\mathbf{C} = \text{blkDiag}(\sigma_{c,1}^2 \mathbf{a}\mathbf{a}^H, \sigma_{c,2}^2 \mathbf{a}\mathbf{a}^H, \dots, \sigma_{c,N}^2 \mathbf{a}\mathbf{a}^H)$, and $\mathbf{N} = \text{blkDiag}(\mathbf{N}_1, \mathbf{N}_2, \dots, \mathbf{N}_N)$. Consequently, we have

$$\begin{cases} H_0 : \mathbf{x} \sim \mathcal{CN}(\mathbf{0}, \mathbf{I}) \\ H_1 : \mathbf{x} \sim \mathcal{CN}(\mathbf{0}, \mathbf{DSD} + \mathbf{I}) \end{cases} \quad (42)$$

where $\mathbf{D} \triangleq (\mathbf{C} + \mathbf{N})^{-\frac{1}{2}} = \text{blkDiag}(\mathbf{D}_1, \mathbf{D}_2, \dots, \mathbf{D}_N)$ with $\mathbf{D}_k \triangleq (\sigma_{c,k}^2 \mathbf{a}\mathbf{a}^H + \mathbf{N}_k)^{-\frac{1}{2}}$ and $\mathbf{x} \triangleq \mathbf{D}\mathbf{r}$. Note that \mathbf{D} and \mathbf{X} in (42) depend on \mathbf{a} . The optimal detector for (42) can be obtained by applying the estimator-correlator theorem as $\sum_{k=1}^N \sigma_k^2 \mathbf{x}_k^H \mathbf{D}_k \mathbf{a}\mathbf{a}^H \mathbf{D}_k (\sigma_k^2 \mathbf{D}_k \mathbf{a}\mathbf{a}^H \mathbf{D}_k + \mathbf{I})^{-1} \mathbf{x}_k \leq \eta$ [38], where η is the threshold, and $\mathbf{x}_k = \mathbf{D}_k \mathbf{r}_k$. Further, $\lambda_k \triangleq \sigma_k^2 \mathbf{a}^H \mathbf{D}_k^2 \mathbf{a}$ and $\theta_k \triangleq \frac{\mathbf{a}^H \mathbf{D}_k \mathbf{x}_k}{\|\mathbf{a}^H \mathbf{D}_k\|_2}$, the canonical form of the detector is $T(\boldsymbol{\theta}) \triangleq \sum_{k=1}^N \frac{\lambda_k |\theta_k|^2}{1 + \lambda_k} \leq \eta$ where $\boldsymbol{\theta} \triangleq [\theta_1 \theta_2 \dots \theta_N]^T$.

V. SIMULATION RESULTS

In this section, simulation results are provided considering a service area of $500 \times 500\text{m}$ with $L = 100$ and K UEs, which are uniformly and independently distributed throughout the region. Every AP comprises $N = 4$ uniform linear array antennas, with a half-wavelength spacing between any two successive antennas. The 2D locations of the APs, UE, and the optimal cluster of APs are illustrated in Fig. 6 (a). The large-scale fading gain is determined by assuming $\Upsilon = -148.1$ dB, $\alpha = 3.76$, $d_{\text{ref}} = 1$ km, and $\sigma_{dB} = 10$ dB [23]. Furthermore, we adopt system configuration as in [8], bandwidth is $B = 20$ MHz and each UE can transmit a maximum of 100 mW power. The path loss for the communication channels is modeled using the 3GPP Urban Microcell model, as defined in [39] and for the sensing channels is modeled using the two-way radar equation. The sensing detection threshold i.e., η is determined according to the false alarm probability of 0.1, which is relevant for radar applications [40].

A. Scalability and need for User Association

To highlight the scalability of CF-mMIMO, it is essential to focus on UA and optimal cluster formation. Early concepts of CF-mMIMO in [24] and [28] faced scalability issues, assuming all APs serving all UEs without limiting the number of UEs each AP could handle. As K grows, this approach becomes impractical, failing to ensure service to all UEs. Each AP would need to compute channel estimates for all K UEs, with infinite complexity as $K \rightarrow \infty$. Moreover, the signal transmission process would imply infinite complexity.

This section will compare the scalability aspect to show the importance of UA and clustering. Fig. 6 (b) illustrates the CDF vs the SE per UE when a) $L = 400, N = 1$ and b) $L = 100, N = 4$ in case of both the proposed scalable UA and non-scalable CF-mMIMO as in [24] and [28]. We compare the proposed scalable distributed MMSE with the non-scalable schemes where all the APs serve all the UEs. The proposed distributed MMSE based UA performs well with an average

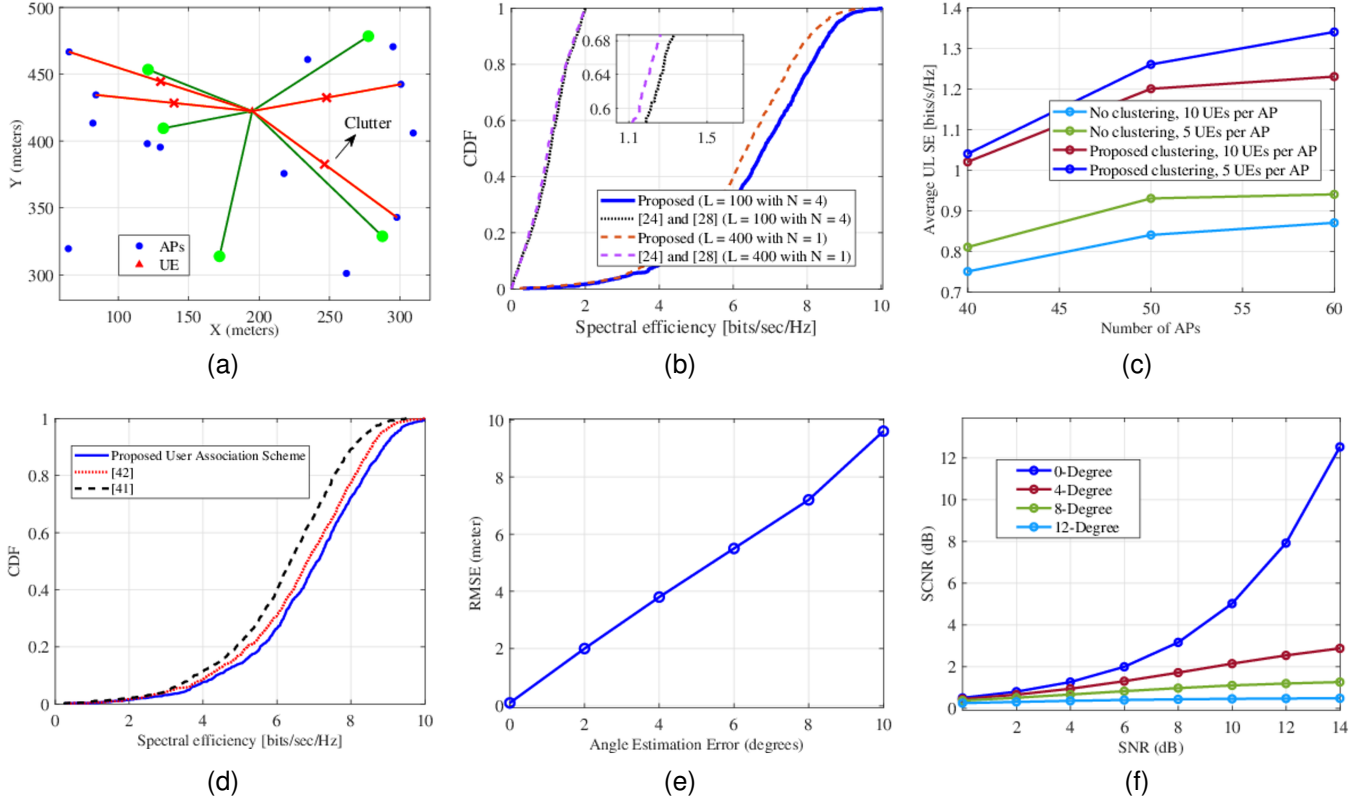


Fig. 6. (a) 2D distribution of the APs, UEs and optimal AP cluster (green circles are the final optimized APs while the APs which have clutter in front of their view angle are represented by the red cross, which are excluded from the final cluster), (b) SE comparison per UE for scalable and non-scalable CF-mMIMO, (c) illustrates the effect of number of APs vs average UL SE for proposed clustering method and for scenario where no clustering is performed, (d) CDF of SE of association schemes, (e) RMSE vs. angle estimation error due to clutter and (f) illustrates SCNR vs SNR for different error in AOA estimation.

SE almost $2.78\times$ higher than the non-scalable CF-mMIMO as can be seen in Fig. 6 (b). The main idea is that the nearest APs capture the majority of the total received power for a specific UE, and these are the APs chosen by our clustering algorithm to serve that UE. Therefore, it is enough to mitigate any interference between the UEs that these APs jointly serve. In non-scalable CF-mMIMO systems, where all APs serve all UEs, significant interference arises. However, this issue is mitigated in scalable systems with UA and clustering.

Moreover Fig. 6 (c) illustrates the UL SE (18), of the system when UA clustering is performed vs when no clustering UA is done, that means non-scalable CF-mMIMO. Without any clustering, increasing the number of APs consistently improves the average user SE, regardless of the number of UEs per AP. However, the proposed clustering schemes, which consider UA clustering, demonstrate significant advantages over the no-clustering approach. As the number of APs increases, the performance gap between the proposed clustering schemes and the no-clustering scenarios becomes more pronounced, highlighting the benefits of the clustering approach in enhancing SE. These findings underscore the importance of opting for UA clustering.

B. Performance of the Initial Phase User Association

In this section, we compare the performance of the initial phase UA, with existing schemes from the literature. Specifically, we evaluate our LSFC scheme against those

presented in [41] and [42]. The CDF of the SE per UE is illustrated in Fig. 6 (d), assuming that $\tau_p = 10$, $K = 50$. The scheme in [41] exhibits the lowest SE per UE among the compared methods. This is primarily because the algorithm may have difficulty identifying APs that can effectively serve multiple UEs with weak channel conditions. Conversely, in [42] associates UEs with weak channel strengths to APs that provide the highest sum of LSFC for the associated UEs across all APs. However, this strategy may not always result in optimal SE performance. Our LSFC scheme outperforms both of these methods, delivering superior SE per UE. This demonstrates the effectiveness of our approach in identifying and leveraging APs with strong channel conditions.

C. Performance of the Second Phase User Association

In this section to show the efficiency of the angulation-based clutter mitigation we measure the performance by RMSE, defined as $RMSE = \sqrt{\frac{1}{Q} \sum_{i=1}^Q \|UE_{estimate}^i - UE_{real}\|^2}$, where Q is the number of measurements for the UEs position. We assume that the AOA measurements were all corrupted by clutter in the environment with different standard deviations. Fig. 6 (e) compares the RMSE performance, this visualization effectively illustrates the impact of angular estimation errors on RMSE in the presence of clutter, emphasizing that larger angular offsets lead to significantly higher RMSE values. This underscores the importance of precise angle estimation to minimize tracking errors in cluttered environments, which is

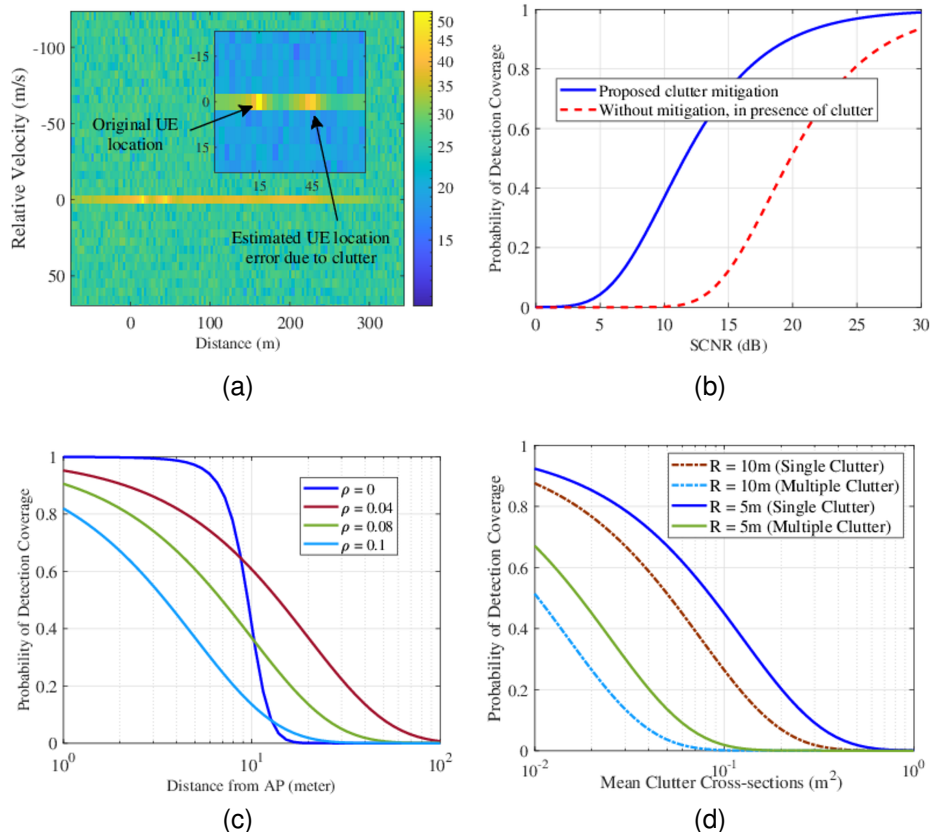


Fig. 7. (a) velocity-distance plot for the original UE location and wrongly estimated target location due to the presence of clutter, (b) Probability of detection coverage vs SCNR, (c) variation of P_{dc} with the UE distance for various clutter densities, keeping the mean clutter cross-section and radar parameters constant and (d) is the variation of P_{dc} with UE distance for different mean clutter cross-sections for single or multiple clutters.

directly related to the clutter present in the surroundings. When the APs have a clear LoS to the UE without any obstructions, the AOA estimation from the radar echo will be more accurate, resulting in a lower RMSE value. By ensuring precise angle estimation through strategic AP-UE pairing, the system can minimize tracking errors and enhance the overall performance in challenging cluttered scenarios.

Furthermore, Fig. 6 (f) illustrates the impact AOA estimation accuracy on the SCNR performance. The different curves represent varying degrees of AOA estimation error, where 0-degree indicates perfect AOA estimation, and 4-degree, 8-degree, and 12-degree denote increasing levels of estimation errors due to clutter in the environment. At lower SNR values, the system with perfect AOA estimation (0-degree) exhibits the highest SCNR, as it can accurately capture the UEs radar parameters. However, as the SNR increases, the scenarios with larger AOA estimation errors start to show degraded SCNR performance compared to the perfect estimation case. This highlights the critical importance of precise AOA estimation, especially in cluttered environments. When the APs have a clear LoS to the UE without obstructions, the AOA estimation from the radar echo will be more accurate, resulting in a higher SCNR and lower RMSE in target tracking. Conversely, in the presence of clutter, the AOA estimation becomes less precise, leading to a lower SCNR and higher RMSE.

D. Performance of the Sensing Detector

Figure 7 (a) illustrates the performance of the optimal sensing detector in tracking UE in the presence of clutter. The velocity-distance plot is based on a binary hypothesis testing framework where the received signal can either consist of clutter and noise H_0 or include the target signal H_1 . The optimal detector, derived using the estimator-correlator theorem, is expressed as a canonical form involving the parameters λ_k and θ_k . In the figure, the original UE location is marked, representing the true position of the target signal. As we can see from the figure, due to clutter, the original location of the UE was 15m away from the AP, but the estimated location shows 45m away, which is a significant error in the range estimation. The estimated UE location, offset from the original due to clutter, highlights this error. This graphical representation not only validates the underlying mathematical model but also highlights the detector's sensitivity to clutter, underscoring the necessity for advanced clutter mitigation techniques to enhance tracking accuracy in complex environments.

E. Radar Detection Coverage Probability

The derived expression for P_{dc} in (25) offers critical insights into UE sensing/tracking performance in a cluttered environment, validated by Fig. 7 (b). This figure shows the impact of clutter on P_{dc} as a function of SCNR, highlighting clutter's degrading effect and the importance of the proposed

clutter mitigation strategy. The clutter-free curve demonstrates nearly perfect detection at higher SCNR levels, with P_{dc} approaching 1 (100%), as clutter effects ($I(R)$) are absent. Conversely, the curve without the proposed mitigation shows significantly affected detection performance, with lower P_{dc} at lower SCNR values, indicating higher false alarm rates and missed detection due to clutter. The reduction in SCNR due to clutter is represented by the integral term ($I(R)$) in the P_{dc} expression, accounting for clutter scatterers' spatial distribution and reflectivity. This underscores the necessity of the proposed UE-AP association strategy to enhance detection in cluttered environments.

F. P_{dc} vs Clutter Density

Figure 7 (c) illustrates how the P_{dc} varies with the distance from the AP for different clutter densities ρ . The mean clutter cross-section and radar parameters are held constant in this scenario. As clutter density increases, the number of scatterers in the environment also rises, leading to more clutter echoes that interfere with the AP sensing detection capabilities. When $\rho = 0$, the environment is free from clutter, resulting in the SCNR being equivalent to the SNR. Consequently, P_{dc} remains high even at larger distances. However, as ρ increases to 0.1, P_{dc} decreases sharply with increasing distance from the AP due to the exponential increase in clutter echoes, which severely impair the AP sensing detection performance. From the perspective of our UA scheme, this indicates that UA needs to account for clutter density to maintain effective sensing performance. As clutter density increases, it becomes crucial to adopt UA strategies to ensure that the UE can still achieve reliable P_{dc} . By incorporating clutter parameters into our association decisions, we can enhance sensing accuracy in cluttered environments.

G. P_{dc} vs Clutter Cross-section

In Fig. 7 (d), the impact of different $v_{c,avg}$ on P_{dc} is shown for both single and multiple clutter reflections, at distances of 5 meters and 10 meters. The figure reveals that increasing $v_{c,avg}$ generally decreases P_{dc} , as larger clutter cross-sections lead to more significant radar signal reflections, thus increasing the interference. For single clutter reflections, the radar's detection performance at 5 meters is superior to 10 meters due to lower path loss and less accumulated clutter effect. However, in scenarios with multiple clutter reflections, the P_{dc} deteriorates more rapidly, especially at greater distances. This is due to multiple reflections exacerbating interference, which makes it more challenging for the AP to detect and track the UE. Consequently, the UA strategy must prioritize including APs in the cluster that provides higher P_{dc} while avoiding APs heavily affected by clutter. This ensures more reliable detection and tracking of the UE, optimizing the performance of the CF-mMIMO system.

VI. CONCLUSION

In conclusion, the proposed UA scheme effectively enhances the performance of JRC CF-mMIMO systems. By seamlessly integrating radar sensing capabilities with the UA process, the scheme optimizes the selection of APs while mitigating the adverse effects of environmental clutter. This approach

addresses the limitations of traditional UA methods, which solely consider communication requirements based AP selection which in return would not necessarily be optimal for sensing. Simulation results validate the efficiency of the proposed JRC-based UA scheme, showcasing its ability to significantly outperform traditional approaches. The scheme's scalability and robustness to dynamic environmental conditions ensure that users are associated with APs that can provide reliable communication links and accurate target tracking. This innovative approach paves the way for enhanced user experience, increased spectral efficiency, and more reliable target tracking, ultimately contributing to the advancement of integrated radar-communication technologies. The proposed scheme optimizes the user-AP pairings by considering the RCS, SCNR, and AOA estimation accuracy, improving overall JRC system performance. Future works may include other parameters of sensing to be incorporated while selecting the APs such as sensing resolution, security aspects, and material characterization, etc.

APPENDIX

PROOF OF THEOREM 2

From the definition of the P_{dc} , we have:

$$P_{dc}(r_t) = \mathbb{P}[\text{SCNR}(r_t) \geq \gamma]. \quad (43)$$

Substituting the SCNR expression under NLoS conditions as

$$P_{dc}(r_t) = \mathbb{P} \left[\frac{\frac{Z v_t e^{-2\alpha' r_t}}{r_t^{2q}}}{n_l + \sum_{c \in \Gamma} \frac{Z G(\theta_c) v_c g_c e^{-2\alpha' r_c}}{r_c^{2q}}} \geq \gamma \right], \quad (44)$$

Rearranging the inequality, we obtain

$$P_{dc}(r_t) = \mathbb{P} \left[v_t \geq \frac{\gamma n_l r_t^{2q} e^{2\alpha' r_t}}{Z} + \gamma r_t^{2q} e^{2\alpha' r_t} \sum_{c \in \Gamma} \frac{G(\theta_c) v_c g_c}{r_c^{2q} e^{2\alpha' r_c}} \right], \quad (45)$$

using the exponential distribution of v_t with mean $v_{t,avg}$ as

$$P_{dc}(r_t) = \mathbb{E}_{v_c, g_c, \Gamma} \left[\exp \left(- \frac{\gamma n_l r_t^{2q} e^{2\alpha' r_t}}{Z} + \gamma r_t^{2q} e^{2\alpha' r_t} \sum_{c \in \Gamma} \frac{G(\theta_c) v_c g_c}{r_c^{2q} e^{2\alpha' r_c}} \right) \right], \quad (46)$$

separating the exponent, we get

$$P_{dc}(r_t) = \exp \left(- \frac{\gamma n_l r_t^{2q} e^{2\alpha' r_t}}{Z v_{t,avg}} \right) \mathbb{E}_{v_c, g_c, \Gamma} \left[\exp \left(- \frac{\gamma r_t^{2q} e^{2\alpha' r_t}}{v_{t,avg}} \sum_{c \in \Gamma} \frac{G(\theta_c) v_c g_c}{r_c^{2q} e^{2\alpha' r_c}} \right) \right], \quad (47)$$

Applying the probability generating functional of the PPP Γ

$$\mathbb{E} \left[\prod_{c \in \Gamma} f(c) \right] = \exp \left(- \rho \int_{\mathbb{R}^2} (1 - f(c)) dc \right), \quad (48)$$

with $f(c) = \exp \left(- \frac{\gamma r_t^{2q} e^{2\alpha' r_t} G(\theta_c) v_c g_c}{v_{t,avg} r_c^{2q} e^{2\alpha' r_c}} \right)$, we get

$$P_{dc}(r_t) = \exp \left(- \frac{\gamma n_l r_t^{2q} e^{2\alpha' r_t}}{Z v_{t,avg}} \right) \exp \left(- \rho \int_{\mathbb{R}^2} \left(1 - \mathbb{E}_{v_c, g_c} \left[\exp \left(- \frac{\gamma r_t^{2q} e^{2\alpha' r_t} G(\theta_c) v_c g_c}{v_{t,avg} r_c^{2q} e^{2\alpha' r_c}} \right) \right] \right) dr_c \right). \quad (49)$$

Assuming $g_c = 1$ (worst-case scenario) and simplifying the expectation inside the integral

$$\begin{aligned} & \mathbb{E}_{v_c} \left[\exp \left(- \frac{\gamma r_t^{2q} e^{2\alpha' r_t} G(\theta_c) v_c}{v_{\text{tavg}} r_c^{2q} e^{2\alpha' r_c}} \right) \right] \\ &= \frac{1}{1 + \frac{\gamma r_t^{2q} e^{2\alpha' r_t} G(\theta_c) v_{c\text{avg}}}{v_{\text{tavg}} r_c^{2q} e^{2\alpha' r_c}}}, \end{aligned} \quad (50)$$

we obtain $= \frac{1}{1 + \frac{\nu'(r_t)G(\theta_c)}{r_c^{2q} e^{2\alpha' r_c}}}$, where $\nu'(r_t) = \frac{\gamma r_t^{2q} e^{2\alpha' r_t} v_{c\text{avg}}}{v_{\text{tavg}}}$.

Substituting back into the integral, we have

$$\begin{aligned} P_{dc}(r_t) &= \exp \left(- \frac{\gamma n_l r_t^{2q} e^{2\alpha' r_t}}{Z v_{\text{tavg}}} \right) \\ & \exp \left(- \varrho \int_0^{2\pi} \int_{r_t}^{r_t + \Delta R} \left(1 - \frac{1}{1 + \frac{\nu'(r_t)G(\theta_c)}{r_c^{2q} e^{2\alpha' r_c}}} \right) r_c dr_c d\theta_c \right), \end{aligned} \quad (51)$$

Simplifying the inner term

$$1 - \frac{1}{1 + \frac{\nu'(r_t)G(\theta_c)}{r_c^{2q} e^{2\alpha' r_c}}} = \frac{\nu'(r_t)G(\theta_c)}{\nu'(r_t)G(\theta_c) + r_c^{2q} e^{2\alpha' r_c}}, \quad (52)$$

we get

$$\begin{aligned} P_{dc}(r_t) &= \exp \left(- \frac{\gamma n_l r_t^{2q} e^{2\alpha' r_t}}{Z v_{\text{tavg}}} \right) \\ & \exp \left(- \varrho \int_0^{2\pi} \int_{r_t}^{r_t + \Delta R} \frac{\nu'(r_t)G(\theta_c) r_c}{\nu'(r_t)G(\theta_c) + r_c^{2q} e^{2\alpha' r_c}} dr_c d\theta_c \right) \end{aligned} \quad (53)$$

Combining the exponents, we have the final result

$$P_{dc}(r_t) = J(r_t) \exp \left(- \frac{\gamma n_l r_t^{2q} e^{2\alpha' r_t}}{Z v_{\text{tavg}}} \right), \quad (54)$$

where

$$J(r_t) = \exp \left(- \varrho \int_0^{2\pi} \int_{r_t}^{r_t + \Delta R} \frac{\nu'(r_t)G(\theta_c) r_c}{\nu'(r_t)G(\theta_c) + r_c^{2q} e^{2\alpha' r_c}} dr_c d\theta_c \right) \quad (55)$$

REFERENCES

- [1] Z. Wei *et al.*, "Integrated sensing and communication signals toward 5G-A and 6G: A survey," *IEEE Internet Things J.*, vol. 10, no. 13, pp. 11 068–11 092, 2023.
- [2] J. G. Andrews *et al.*, "Are we approaching the fundamental limits of wireless network densification?" *IEEE Communications Magazine*, vol. 54, no. 10, pp. 184–190, 2016.
- [3] S. Parkvall *et al.*, "NR: The new 5G radio access technology," *IEEE Communications Standards Magazine*, vol. 1, no. 4, pp. 24–30, 2017.
- [4] S. Chen *et al.*, "A survey on user-centric cell-free massive MIMO systems," *Digital Communications and Networks*, vol. 8, no. 5, pp. 695–719, 2022.
- [5] Ö. T. Demir *et al.*, "Foundations of user-centric cell-free massive MIMO," *Foundations and Trends® in Signal Processing*, vol. 14, no. 3-4, pp. 162–472, 2021.
- [6] H. Q. Ngo *et al.*, "Cell-free massive MIMO: Uniformly great service for everyone," in *IEEE 16th international workshop on signal processing advances in wireless communications*. IEEE, 2015, pp. 201–205.
- [7] J. Fang *et al.*, "Cell-free mMIMO systems in short packet transmission regime: Pilot and power allocation," *IEEE Trans. Veh. Technol.*, vol. 73, no. 6, pp. 8322–8337, 2024.
- [8] E. Björnson *et al.*, "Scalable cell-free massive MIMO systems," *IEEE Trans. Commun.*, vol. 68, no. 7, pp. 4247–4261, 2020.
- [9] S. Buzzi and C. D'Andrea, "Cell-free massive MIMO: User-centric approach," *IEEE Wireless Commun. Lett.*, vol. 6, no. 6, pp. 706–709, 2017.
- [10] S. Chen *et al.*, "Structured massive access for scalable cell-free massive MIMO systems," *IEEE J. Sel. Areas Commun.*, vol. 39, no. 4, pp. 1086–1100, 2020.
- [11] H. Q. Ngo *et al.*, "On the performance of cell-free massive MIMO in rician fading," in *52nd Asilomar Conference on Signals, Systems, and Computers*. IEEE, 2018, pp. 980–984.
- [12] M. Sarker *et al.*, "Access point-user association and auction algorithm-based pilot assignment schemes for cell-free massive MIMO systems," *IEEE Syst. J.*, vol. 17, no. 3, pp. 4301–4312, 2023.
- [13] C. D'Andrea *et al.*, "User association in scalable cell-free massive MIMO systems," in *54th Asilomar Conference on Signals, Systems, and Computers*. IEEE, 2020, pp. 826–830.
- [14] Z. Behdad *et al.*, "Multi-static target detection and power allocation for integrated sensing and communication in cell-free massive MIMO," *IEEE Trans. Wireless Commun.*, 2024.
- [15] Z. Behdad, Ö. T. Demir *et al.*, "Joint processing and transmission energy optimization for ISAC in cell-free massive MIMO with URLLC," *arXiv preprint arXiv:2401.10315*, 2024.
- [16] M. Elfiatoure *et al.*, "Multiple-target detection in cell-free massive MIMO-assisted ISAC," *arXiv preprint arXiv:2404.17263*, 2024.
- [17] W. Mao *et al.*, "Beamforming design in cell-free massive MIMO integrated sensing and communication systems," in *GLOBECOM IEEE Global Communications Conference*. IEEE, 2023, pp. 546–551.
- [18] W. Mao, Lu *et al.*, "Communication-sensing region for cell-free massive MIMO ISAC systems," *IEEE Trans. Wireless Commun.*, 2024.
- [19] J. Xu *et al.*, "Hybrid index modulation for dual-functional radar communications systems," *IEEE Trans. Veh. Technol.*, vol. 72, no. 3, pp. 3186–3200, 2023.
- [20] Z. Xiao *et al.*, "Waveform design and performance analysis for full-duplex integrated sensing and communication," *IEEE J. Sel. Areas Commun.*, vol. 40, no. 6, pp. 1823–1837, 2022.
- [21] X. Ma *et al.*, "Cooperative beamforming for RIS-aided cell-free massive MIMO networks," *IEEE Trans. Wireless Commun.*, vol. 22, no. 11, pp. 7243–7258, 2023.
- [22] S. Gopi *et al.*, "Cooperative 3D beamforming for small-cell and cell-free 6G systems," *IEEE Trans. Veh. Technol.*, vol. 71, no. 5, pp. 5023–5036, 2022.
- [23] E. Björnson *et al.*, "Massive MIMO networks: Spectral, energy, and hardware efficiency," *Foundations and Trends® in Signal Processing*, vol. 11, no. 3-4, pp. 154–655, 2017.
- [24] H. Q. Ngo *et al.*, "Cell-free massive MIMO versus small cells," *IEEE Trans. Wireless Commun.*, vol. 16, no. 3, pp. 1834–1850, 2017.
- [25] E. Björnson *et al.*, "Massive MIMO networks: Spectral, energy, and hardware efficiency," *Foundations and Trends® in Signal Processing*, vol. 11, pp. 154–655, 01 2017.
- [26] J. Park *et al.*, "Downlink cell-free massive MIMO with pilot contamination," *IEEE Trans. Veh. Technol.*, vol. 73, no. 1, pp. 1412–1417, 2024.
- [27] A. Sesyuk *et al.*, "Radar-based millimeter-wave sensing for accurate 3-D indoor positioning: Potentials and challenges," *IEEE Journal of Indoor and Seamless Positioning and Navigation*, vol. 2, pp. 61–75, 2024.
- [28] E. Nayebi *et al.*, "Performance of cell-free massive MIMO systems with MMSE and LSFDR receivers," in *2016 50th Asilomar Conference on Signals, Systems and Computers*, 2016, pp. 203–207.
- [29] S. N. Chiu *et al.*, *Stochastic geometry and its applications*. John Wiley & Sons, 2013.
- [30] M. I. Skolnik *et al.*, *Introduction to radar systems*. McGraw-hill New York, 1980, vol. 3.
- [31] T. L. N. Nguyen *et al.*, "A new approach for positioning based on AOA measurements," in *International Conference on Computing, Management and Telecommunications*. IEEE, 2013, pp. 208–211.
- [32] J. Yin *et al.*, "A simple and accurate TDOA-AOA localization method using two stations," *IEEE Signal Process. Lett.*, vol. 23, no. 1, pp. 144–148, 2016.
- [33] A. Naem *et al.*, "Polarization-based multiplexing: Enabling spectrum efficient joint radar and communication," *IEEE Wireless Commun. Lett.*, vol. 13, no. 5, pp. 1414–1418, 2024.
- [34] J. C. L. Fish, *Coordinates of elementary surveying*. The author, 1909.
- [35] J. Stewart, *Calculus, Early Transcendentals*, AP ed. Cengage Learning, 2011.
- [36] X. Qiao *et al.*, "Two-layer large scale fading precoding for cell-free massive MIMO: Performance analysis and optimization," *IEEE Trans. Veh. Technol.*, vol. 73, no. 3, pp. 3901–3916, 2024.
- [37] M. M. Naghsh *et al.*, "Unified optimization framework for multi-static radar code design using information-theoretic criteria," *IEEE Trans. Signal Process.*, vol. 61, no. 21, pp. 5401–5416, 2013.
- [38] S. M. Kay, "Statistical signal processing, volume II, detection theory," 1998.

- [39] 3GPP, “Further advancements for E-UTRA physical layer aspects (release 9),” 3GPP, Tech. Rep. TS 36.814, 2017.
- [40] S. Guruacharya *et al.*, “MAP ratio test detector for radar system,” *IEEE Trans. Signal Process.*, vol. 69, pp. 573–588, 2020.
- [41] S. Chen *et al.*, “Structured massive access for scalable cell-free massive MIMO systems,” *IEEE J. Sel. Areas Commun.*, vol. 39, no. 4, pp. 1086–1100, 2021.
- [42] M. Sarker *et al.*, “Granting massive access by adaptive pilot assignment scheme for scalable cell-free massive MIMO systems,” in *IEEE 93rd Vehicular Technology Conference*, 2021, pp. 1–5.